GEOTECHNICAL REPORT

ANALYSIS OF ~~THE CONDITIONS THAT WOULD CAUSE HYDROGEOLOGICAL~~SLOPE INSTABILITY CONDITIONS IN THE KHINIS ARCHAEOLOGICAL AREA. MODELLING OF ACTIVE PROCESSES AND PRELIMINARY PROPOSALS FOR A SITE PRESERVATION PLAN

DR EMILIANO DI LUZIO

CNR ITABC, INSTITUTE FOR TECHNOLOGY APPLIED TO CULTURAL HERITAGE

1 INTRODUCTION

This technical-scientific report describes the methods used and results obtained for an evaluation of the conditions of ~~hydrogeological~~ slope instability affecting the archaeological area of Khinis (Iraqi Kurdistan), which constitute a danger for safeguarding and protecting the local cultural heritage and its fruition by visitors.

Land surveys have enabled us to understand the geological structure of the territory and gather the information necessary for the determination of the ~~gravitational~~ gravity-driven instability processes acting on some rock ~~walls~~escarpments, including those on the surface of which bas-reliefs dating to700 BC have been sculpted.

By means of analysis of the fractured, discontinuous-type rock bodies, focused on evaluating the characteristics of the discontinuity systems that ~~pass through~~affect the local geological sequence, it was possible to construct geometric and dynamic models of the stability conditions of some discrete rock volumes (i.e. isolated by ~~the~~ main discontinuities). With the aid of aerial photogrammetric surveys, the dimensions and volumes of these elements were calculated and the potential type of kinematic failure mechanism was defined. Lastly, the results of the stability analyses permitted an evaluation of the equilibrium conditions between the active forces and the resistant forces (the limit~~ing~~ equilibrium) and to propose some measures that may be taken so as to mitigate the risk of collapse. The stability conditions are also discussed in relation to factors that might potentially trigger collapses, such as seismic vibration and rainwater infiltration.

In addition, an analysis was conducted of processes of rock~~-~~fall from the rock faces present on the upper part of the Khinis slope – above the series of bas-reliefs, which are close to the valley floor. Using probabilistic and kinematic 3D modelling of the propagation trajectories obtained with ROTOMAP® software produced by GeoSoft International (**Scioldo, 1991; 2006**), spatial distribution maps were obtained over the slope for motion parameters such as velocity, kinetic energy and height from the ground. Combined with the estimates of the "design block" – i.e. a projected block representing the phenomenon – the results of the modelling allowed the planning of countermeasures designed to control and ~~contain~~ mitigate the collapse process, based on the installation of suitable rockfall barriers.

2. THE LOCAL STRUCTURAL GEOLOGY AND EVIDENCE OF INSTABILITY

The geological sequence that outcrops in the Khinis area consists of well-stratified calcarenites, i.e. clastic sedimentary rocks, largely calcareous with regard to chemical composition.

This sedimentary ~~succession~~ sequence is folded into a large E-W monocline that ~~descends~~ dips southwards with an average slope of 15°. The calcarenites form strata that are metres or decimetres in thickness, as well as massive deposits up to 15-20 metres thick. The relief carvings are located on the eroded faces of the latter. The thickest strata are present in the ~~central~~ middle portion of the slope, where the calcarenite sequence is well exposed (**Figure 1**).

Figure 1. View of the locale calcarenitice sequence ~~(a monocline).~~

The rock mass is affected by mechanical discontinuities associated with the ~~stratification~~ bedding (S0) and with a weak tectonic deformation that includes groups of joints and mega-joints, namely widely-spaced cracks of considerable length, metres or decametres (**Figure 2a**). The discontinuities are more numerous near the slope where the bas-reliefs are located, where the prevailing joint system is oriented NNE-SSW and characterized by a limited number of regularly-spaced features (about 10 m apart), of

considerable length (up to 100 m) and vertical or sub-vertical. Another system of shorter NW-SE joints shows a greater concentration on the hillside facing a disused quarry. Lastly, the picture is completed (**Figure 2b**) by some WNW-ESE aligned discontinuities, less numerous and concentrated in the western sectors.

The kinematic characterization of tectonic features was not among the objectives of this study. However, there is evidence that suggests that the joint systems are linked to strike-slip tectonics ~~movements~~. In fact the planes of discontinuity have always a high cut-off (intersection) angle with the strata (S0), and are closed or present apertures only several millimetres wide, and are not associated with appreciable vertical dislocations in the bedding planes, which are uninterrupted. It follows that movement of the rock masses may have taken place in a direction parallel to that of the tectonic features. Several discontinuities which, on the contrary, have significant openings, especially when close to the hillsides, may instead have originated and evolved as a result of lateral load reduction due to active and retrograde collapse processes on the slope.

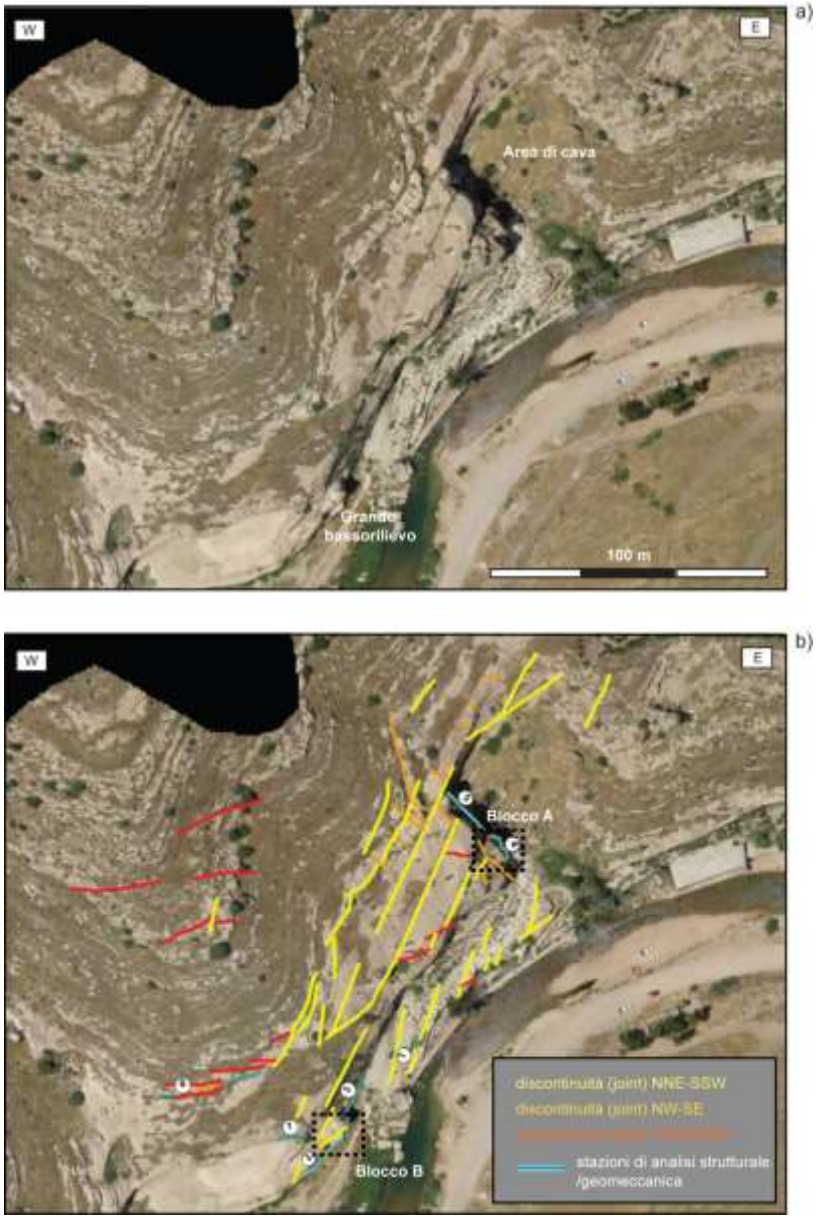

Figure 2. a) Satellite photograph of the area; b) Structural ~~plan~~ map of the area under study, showing main joint systems, position of structural analysis stations 1-7 and rock ~~masses~~ blocks A and B.

The rock face on which the bas-reliefs were made presents clear and significant signs of instability, due to gravity-driven processes with different characteristics ~~that evolve differently~~. The presence of mega-joints and very thick strata leads to the isolation of potentially unstable blocks of considerable volume within the rock mass, of the order of hundreds of m^3, as explained below. In this report the stability conditions ~~of~~ will be analyzed of a first block (A) located at the SW edge of the disused quarry area located inside the archaeological park, and of a second block (B) containing the large rock-face bas-relief (**Figures 2 and 3**).

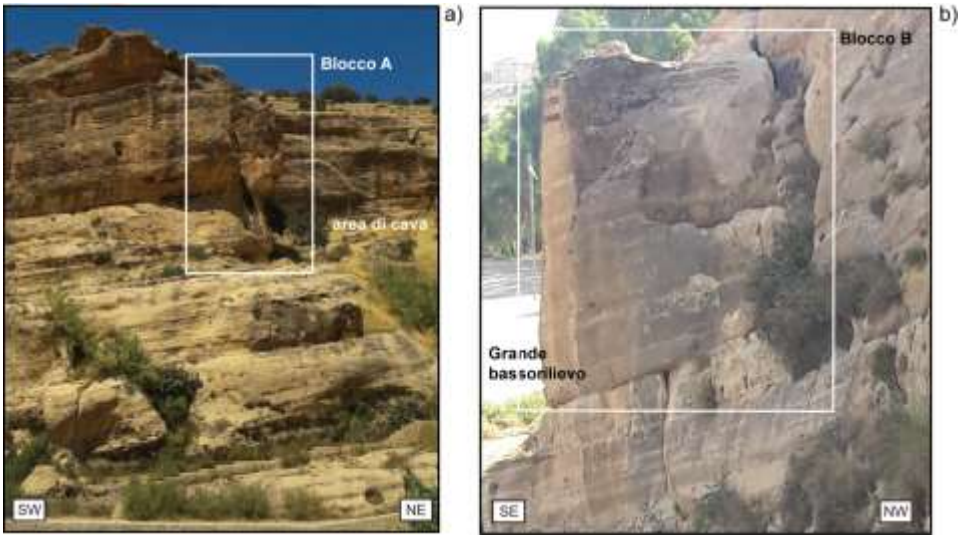

Figure 3. Rock ~~masses~~ blocks A and B defined by the intersection of joints and bedding pla~~i~~nes

In addition to this type of localized instability, the Khnis area is subject to widespread rockfall phenomena deriving from the small ~~slopes~~ rock escarpments (H = 2-3 metres) ~~that are widespread~~ on the middle and upper parts of the slope (**lines 1, 2 and 3 in Figures 4a-c**). After detachment and fall, the ~~loose~~ rock~~s~~ blocks can travel down the slope. Indications of this process are the numerous blocks observed on the sloping hillside above the bas-reliefs; these came from scarp lines 2 and 3, and did not have enough energy to roll further towards the valley floor. As will be discussed below, the probabilistic model created for the simulation of the trajectories is based on a georeferenced inventory of the rock~~s~~ blocks ~~present~~ documented on the slope.

The possibility that limestone blocks detached from the higher rock faces (lines 1, 2 and 3) could descend as far as the stream – and thus strike the part of the archaeological area in front of the bas-

reliefs – could not be ruled out *a priori*. Moreover it was evident before the modelling that scarp line 1, overlooking the large bas-relief, contained potentially unstable boulders capable of reaching the ground surface beneath directly in the free-fall phase.

Figure 4. a) View of the hillside above the rock face with bas-reliefs and high scarp lines 1,2 and 3; b),c) stone blocks in static equilibrium on the hillside near scarp line 2

3 ~~ROCK BODY~~ GEOMECHANICS OF ROCK MASSES AND ANALYTICAL METHODS

3.1 Fractured ~~bodies of~~ rock masses

A 'rock mass~~body~~' is defined as a volume of intact rock (stone matrix) together with the mechanical discontinuities of various origins which, to a greater or lesser extent, interrupt its continuity. The physical behaviour of a rock ~~body~~ mass therefore depends on the overall resistance characteristics of the ~~rock~~ matrix and the discontinuities combined. The relative weight of these two factors depends upon the intensity of fracturing, commensurate with the scale of the problem under examination, and the conditions of stress in situ.

In general there are two approaches to problems related to case studies of fractured rock ~~bodies~~masses. In the first type the body is considered as a discontinuous medium in which movement can take place exclusively along the discontinuities, while in a second group of methodologies the body is approximated to a continuous volume and its behaviour is described by overall qualitative or semi-quantitative parameters.

In order to follow the first approach it is necessary to know precisely the geometric-spatial characteristics of the discontinuities, and to make an estimate of the residual shear strength along the possible failure planes. A common feature of discontinuity surfaces is a negligible tensile strength, and shear strength values significantly lower than those of intact rock. In the second type of approach, on the other hand, empirical classifications are generally used, which are able to provide commonly-used design parameters that have demonstrated their validity and applicability to concrete situations over the years.

The choice of one approach or the other is strongly conditioned by the conditions of the rock body under examination, and by the questions to which answers are sought. In the case of the Khinis hillsides, the fracture ~~complex~~ network affecting the local geological ~~succession~~ sequence includes only a few marked discontinuities of great extension – even tens of metres in length – and spaced one to several metres apart. It follows that such discontinuities may have an important role with regard to the behaviour of the rock body that contains them; their geometric characteristics and resistance govern the conditions of stability or instability of the individual rock volumes that are bounded by them. In this study we have therefore chosen to adopt a 'discontinuous' approach and to carefully evaluate the parts played by mechanical discontinuities (joint systems and S0 ~~stratification~~).

In order to survey the rock slope ~~terrain~~ at Khinis it was decided to adopt an objective criterion by measuring discontinuities along 7 scan-lines (**Figure 2b**). However, particular attention was paid to examining the geometrical characteristics of those discontinuities that from field observation ~~of the terrain~~ seemed to play an important part in conditioning the stability of the stone blocks.

For a description of the measurements and observations made of the discontinuities present in the rock bodies at Khinis, see the international ISRM standard (2007). Only the most significant features regarding the spatial and ~~mechanical~~ strength characterization of the discontinuity surfaces are described below.

3.2 Principal distinguishing parameters of joints and discontinuity systems.

3.2.1 Orientation

The orientation or position of a plane in space is defined by two measurements: i) the dip direction, i.e. the horizontal projection of the direction of maximum slope of the plane. This is defined by the angle α (clockwise) of the projection with respect to magnetic north. The dip direction is always perpendicular to the intersection between the measured plane ~~in question~~ and the horizontal plane (i.e. the direction of the plane); ii) the dip angle, ~~i.e. the slope~~ indicated by the angle β. Using similar parameters it is also possible to define, for a line in space, the dip direction α, the dip angle β and the pitch γ (the angle measured on the inclined plane between the line and the direction of the plane on which it lies (**Figure 5**).

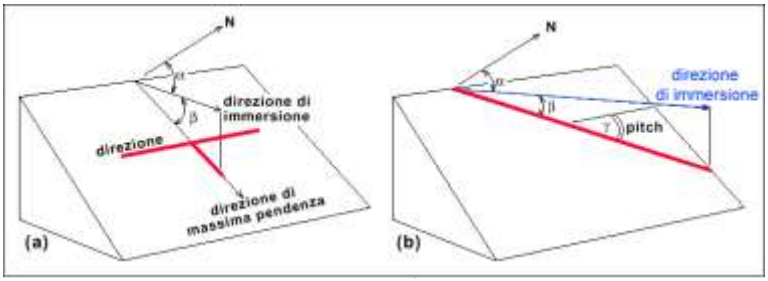

Figure 5. Parameters for measuring the orientation of a) a plane and b) a line in space

The positions of planes and lines within rock masses are represented in structural geology and in geomechanics using stereographic projections (**Figure 6**). A line (**Figure 6a**) or plane (**Figure 6b**) are imagined to intersect a projected hemisphere, giving rise to a point (**Figure 4c**) or a continuous curved line (**Figure 4d**), respectively. The stereographic projection of the point or curved line onto the hemisphere's equatorial plane gives rise in turn to a "pole" (**Figure 6e**) or a cyclograph (**Figure 6f**). In the image on the right in **Figure 6** several cyclographs are shown, which represent all planes in the N-S direction but with different inclinations, ranging from 0 ° (horizontal plane) to 90 ° (vertical plane). **Figure 7a** shows several cyclographs which represent planes with different orientations and dip angles~~slopes~~. **Figure 7b** illustrates the method of representing the "pole" of a plane. This derives from a line perpendicular to the plane itself and the projection, again on the hemisphere's equatorial plane, of the point of intersection between the aforementioned line and the hemisphere itself.

ha formattato: Tipo di carattere: Grassetto

ha formattato: Colore carattere: Automatico

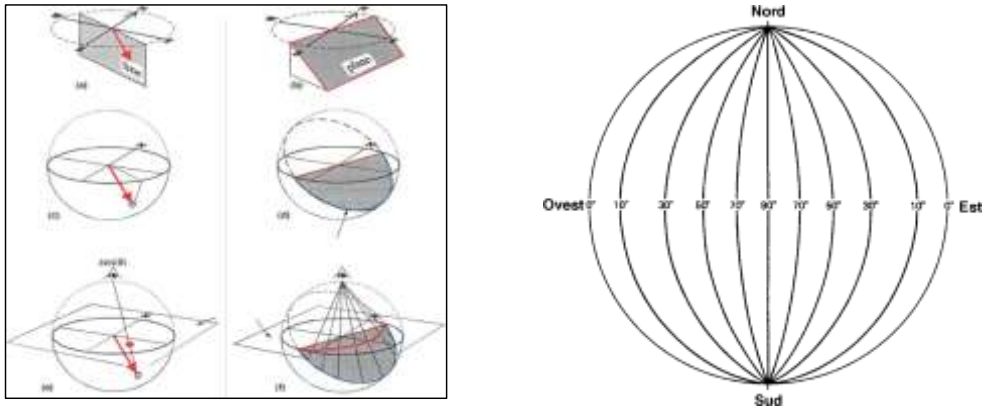

Figure 6. Principles of stereographic projection

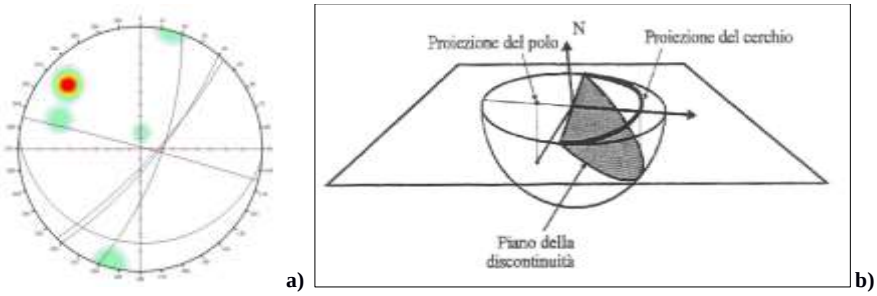

a) **b)**

Figure 7 a) Examples of cyclographs representing planes with different orientations and dips, b) method of representing the pole of a plane.

3.2.2 Roughness

The roughness ~~or unevenness of the faces of~~ discontinuities is an important characteristic for evaluating the amount of resistance along the failure planes, since this influences the forces ~~of cohesion~~ that contrast instability processes. It is generally characterized by main undulations at the ~~scale of the~~ outcrop scale and by actual roughness at a larger scale. The undulation is hardly appreciable in an outcrop (except for macroscopic manifestations), while the roughness can be evaluated by means of a method proposed by **Barton and Choubey, (1977)** using a profilometer (also called *Shape Tracer* ~~or comb by Barton~~). In practice this instrument reproduces the profile of the faces of discontinuities along a 10 cm section. This profile can be compared with those shown in a table of ten standard profiles (**Figure 8**). Each of the ten standard profiles corresponds to a roughness index (JRC - Joint Roughness Coefficient) ranging from 0 (perfectly smooth surface) to 20 (extremely rough surface).

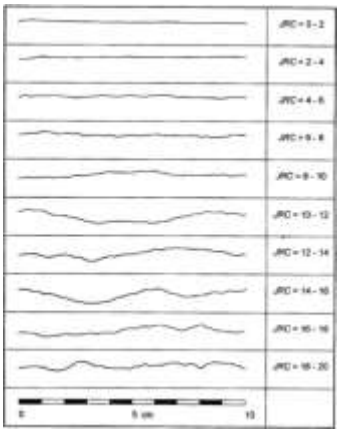

Figure 8. Surface roughness profiles of discontinuities and relative JRC values.

3.2.3 Discontinuity wall surface ~~resistance~~strength

The uniaxial compressive strength of the surfaces of discontinuities ~~and~~ can be estimated by means of sclerometric tests carried out in the field on rock outcrops using a ~~rebound hammer or~~ Schmidt Hammer. This instrument measures the rebound height of a known mass on discontinuity rock faces. The rebound distance is defined using an index that is proportional to the uniaxial compressive strength of the rock. By measuring the rebound of the mass after impact, the inelastic absorption of the rock may be estimated – and hence its impact ~~resistance~~ strength as indicated on the correlation table shown in **Figure 9**~~.~~)~~F~~for the calcarenites of the Khinis geological succession a density value of 2.4 g/cm^3 was ~~recorded~~assumed).

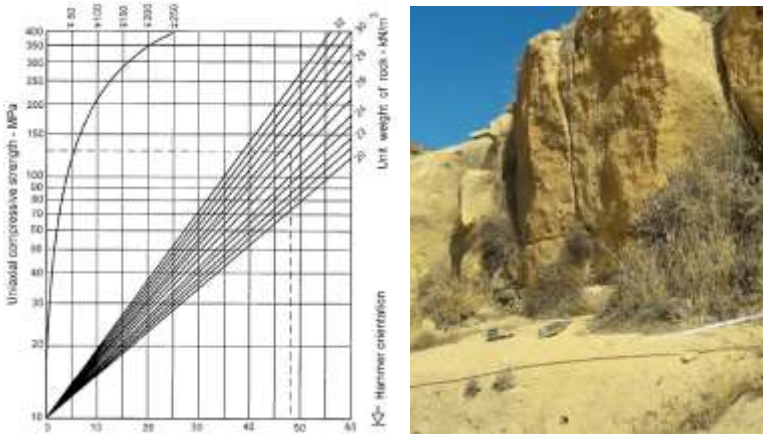

Figure 9. Schmidt Hammer correlation chart, and the use of the instrument *in situ* on a rock layer.

For a given surface ~~resistance~~strength, the reading is lowest when the hammer is used vertically downwards (rebound against gravity) and highest when vertically upwards. **Table 1** gives corrections to be applied when the hammer is used in directions other than straight downwards.

rebound	downwards		upwards		horizontal
	-90°	-45°	+90°	+45°	0°
10	0,0	-0,8	-	-	-3,2
20	0,0	-0,9	-8,8	6,9	-3,4
30	0,0	-0,8	-7,8	-6,2	-3,1
40	0,0	-0,7	-6,6	-5,3	-2,7
50	0,0	-0,6	-5,3	-4,3	-2,2
60	0,0	-0,4	-4,0	-3,3	-1,7

Table 1. Correction values (r) for Schmidt Hammer readings when it is not used vertically downwards (-90°).

3.3 Criterion used to estimate discontinuity ~~resistance~~ strength parameters

Study of the mechanical behaviour of discontinuities is based on the relationship between the ~~end on~~shear ~~forces~~ stress applied and the tangential ~~movement~~ displacement produced. **Barton and Choubey (1977**) used an empirical criterion derived from the behaviour of discontinuities measured in laboratory tests, which allows the ~~resistance~~ strength parameters of rough discontinuities to be measured using the formula:

where:

$$\tau' = \sigma'_n \tan [\, JRC \cdot \log_{10}(JCS/\sigma'_n) + \varphi_r \,]$$

τ'= effective tangential force acting on the discontinuity;

σ'n: effective normal force acting on the discontinuity;

φr: residual angle of ~~attrition~~friction;

JRC: Joint Roughness Coefficient;

JCS: Joint wall Compression Strength.

The criterion suggests that the resistance of a discontinuity depends upon three fundamental components: a~~n~~ friction component (φr), a geometrical component expressed through surface roughness (JRC), and a component that described the resistance to breakage of asperities (JCS/σ'n).

As seen above, JCS values may be obtained from sclerometric measurements on joint faces (JCS expressed in MN/m^2), while the JRC coefficient varies from 1 to 20 and may be obtained by comparing joint roughness profiles with standard profiles with known corresponding JRC values.

The equation proposed by **Barton and Choubey (1977)** for the estimation of the residual angle of attrition φ_r of

ha formattato: Pedice

an altered joint discontinuity is:

$$\phi_r = (\phi_b - 20°) + 20\ (r/R)$$

where:

φ_b = basic friction angle ~~of attrition~~, i.e. the angle of ~~attrition~~friction for perfectly smooth ~~surfaces~~, polished, not rough surfaces; -for ~~a~~the Khinis calcarenites a reference value of φ_b = 30° may be used (**Hoek and Bray, 1981; Cruden and Hu, 1988; Bruce et al., 1989; Goodman 1989; Gonzalez de Vallejo et al., 2005; Waltham, 2009)**

ha formattato: Pedice

ha formattato: Pedice

r = ~~value of~~ number of Schmidt Hammer rebounds on an altered surface

R = ~~value of~~ number of Schmidt Hammer rebounds on a fresh surface, where R>r

3.4 ~~Methods of~~Slope stability evaluation using ~~at~~ limit~~ing~~ equilibrium method.

The limit~~ing~~ equilibrium method is ~~by far that used most frequently in stability analysis in the field of geotechnics. It is~~ applied in cases where it may reasonably be supposed that a volume of unstable terrain or rock may be considered rigid without taking into account internal deformation or movements, and when the fracture surface is evident and well-defined a priori. These are obviously two simplifying assumptions with regard to a slope system, since a slope's degree of stability is also linked to the internal stress-strain conditions~~deformations it manifests~~, ~~whereas this method only requires determination of the material's resistance criteria along a fracture surface.~~

In practice, the method consists of the calculation of: i) the forces acting along a predefined sliding surface, ii) the resistance posed to failure by the surface itself~~,~~. ~~and t~~The definition of a Safety Factor (Fs) is given by the ratio ~~between the first two (Fs = resistant~~ resisting forces / acting forces~~)~~ ~~that~~ and is assumed to be constant along the whole potential ~~sliding~~ failure surface.

The condition of limit~~ing~~ equilibrium is obtain~~s~~ed when the ~~active~~ acting (or driving) forces are equal to the resisting~~ant~~ forces: in this circumstance the ~~resistance~~ strength of the terrain or ~~stone~~ rock block is completely engaged over the entire surface and the slope is on the point of collapse.

To complete the calculation of a limit~~ing~~ equilibrium solution it is first necessary to identify a "breakage mechanism" of a slope or ~~stone~~ rock block, as in the case of Khinis. This can be done once the mechanical discontinuities that isolate the block inside the rock mass are acknowledged as ~~, and which of these constitutes a~~ potential failure plane~~s~~.

For these operations, commercial~~ly~~ softwares ~~available~~ for limit~~ing~~ equilibrium calculation ~~software~~ w~~as~~ere used in this report (**Figure 10**), that enabled potentially unstable rock bodies to be distinguished and the geometry of the sliding surfaces reconstructed in relation to the stable rock volumes.

Figure 10. Representation of a rigid block sliding on a planar surface and calculation of geometric and ~~resistance~~ strength parameters and safety factor Fs.

Lastly, it must be remembered that an initially stable slope (Fs > 1) may become unstable for two reasons:
- an increase in the forces acting on the ~~break~~ failure surfaces caused by an increase in load (e.g. due to construction work or a seismic event), or an increase in slope inclination (due for example to erosion or excavation at the base);
- a decrease in the resisting forces due to an increase in interstitial water pressure (~~raising of the water table,~~ percolation along the discontinuity surfaces, reduction of capillary tension etc.) or due to the effect of physical, chemical or biological alteration phenomena.

4 METHOD FOR SIMULATING ROCK-FALL PROCESSES IN THE KHINIS AREA.

Commentato [i1]: Always use rockfall not rock fall

The rock~~y~~ slope above the rock face with bas-reliefs at Khinis contains a number of scarps affected by joint systems with narrower ~~gaps~~ spacing than those that delimit blocks A and B. These ~~slopes~~ escarpments ~~may~~ give rise to ~~active~~ rock-falls ~~processes~~ as evidenced by the presence of several erratic boulders ~~on the~~ downslope, lying in zones that are less steep (**Figures 4b-c**). Our analysis of these processes has the objective of assessing the real risk that these instabilities might also involve the foot of the hill and valley, which would constitute a great danger for the public fruition of the archaeological site.

In order to evaluate the kinematic and dynamic parameters of this phenomenon, and thus be able to plan the most appropriate protective measures for the safety of the area beneath the slope, a study was performed of the potential trajectories of blocks subject to collapse phenomena. The simulations were completed using the ROTOMAP calculation program, which has been employed in numerous case studies ~~in~~and ~~diverse~~ different geological ~~circumstances~~ scenarios (e.g. **Del Maschio et al., 2007**; **Bourrier et al. 2009**; **Ferrari et al., 2013**)

The software adopts a statistical-probabilistic approach, furnishing numerous simulations of ~~descents~~rock block trajectories, which are generated after the initial motion parameters and the coefficients of elastic restitution and dynamic friction along the slope have been defined. The probabilistic approach provides a ~~remedy~~ solution to the problem of the indeterminacy of ~~the values of the~~ motion ~~parameters~~ variables ~~of each individual slope~~ by randomly varying the input ~~motion~~ parameters (initial conditions, elastic ~~return~~ rebound coefficients, dynamic friction angle etc.). The modelled outputs must then be compared with the observed real-life conditions (Monte Carlo statistical method). A “back analysis” procedure is therefore adopted, with a weighted variation of the initial model parameters – limited, however, to values suggested in the literature – until a simulated distribution of collapsed blocks that is similar to that actually observed on the field is obtained.

The probabilistic model used by the ROTOMAP software employs a "lumped mass" approach, i.e. it represents a falling block as a point in space where its mass is concentrated (dimensionless mass) and which possesses velocity (**Azzoni et al., 1995)**. The software produces three-dimensional fall trajectories that start from the scarp lines identified in the field, with subsequent rolling and bouncing down the slope. Finally, ~~T~~the topography of the hillside is represented as a further model input by a grid raster surface consisting of the spatial reconstruction of a series of 3D elevation points ~~recorded in the field~~ (**Figure 11**).

Figure 11. Representation of the starting lines and points of the rockfall simulations (lines 1-3) and ~~positions~~ distributions of topographic grid points ~~measured in the field~~.

Analysis of rock-fall movement makes reference to a theoretical model applicable to each individual block that detaches from the rock face. The types of motion which a boulder may undergo on a given slope sector are: 1) free -fall; 2) rebound; 3) rotational sliding.

A free fall phase occurs when the face from which the block become detached is sub-vertical or juts out. After this initial phase, the simulation starts the blocks from launching positions arranged along ~~broken~~ lines coinciding with the scarp base, with variable V_0 velocities depending on the height of the detaching points on the escarp~~s~~ment. The calculation of each block's starting speed is based on the route taken in this first free fall phase down the rock face; h1 and h2 refer to the differences of minimum and maximum altitude between the possible detachment points on the scarp and the scarp base, and the minimum and maximum initial speeds are obtained according to the formula for uniform accelerat~~ing~~ed ~~uniform~~ motion V_{0i}=$Cs\sqrt{2gh_i}$ (**Figure 12**). Cs is a correction factor (from 0 to 1) that takes account of possible inelastic rebounds~~shocks~~ during the phase of free fall down scarps that are not exactly vertical, which will reduce V_0.

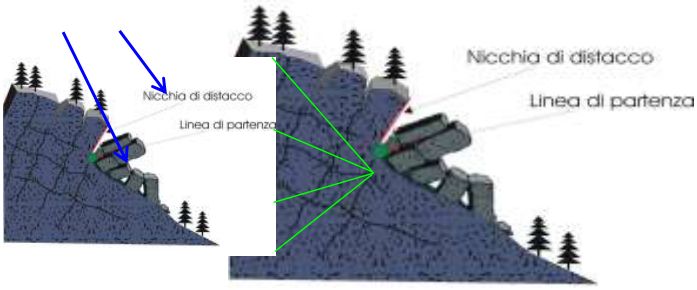

Figure 12: Start lines (green) located at the base of the detachment scarp (red);

h1 indicates the minimum height and h2 the maximum height of possible detachments.

Since a stochastic approach is used, a significant number of the initial motion conditions ~~employed in the simulation~~ generate different simulated paths. The variables involved are: the number of starting points (Nsp~~p~~) on the slope; the number of starting ~~speeds~~ velocities at each point (Nvp), a function of the variable height of detachment; the number of possible angular variations of the ~~rolling~~motion direction with respect to the maximum slope line of the hillside (N~~v~~av).

The total number of detachments and descents obtained in a simulation is then calculated by the product of these:

n° descents = (N~~p~~sp) x (Nvp) x (N~~v~~av)

After free fall and departure, at each impact (rebound) on the slope the evaluation of the kinetic energy lost by the boulder during the impact is defined by the tangential and normal ~~return~~ restitution coefficients Kn and Kt. The elastic ~~return~~ restitution coefficient is defined as: $K = (v_b / v_a)$

where:

v_b = block velocity after impact; v_a = block velocity before impact.

K has values 0-1: K = 0 when an impact in completely inelastic; K = 1 when an impact in perfectly elastic.

In the modelling the coefficient K is normally split into its two components K_n - normal - and K_t - tangential (**Figure 13**).

K_n = Coefficiente di restituzione normale
K_t = Coefficiente di restituzione tangenziale
Va_n = Componente normale della velocità prima dell'urto (Va)
Vb_n = Componente normale della velocità dopo l'urto (Vb)
Va_t = Componente tangenziale della velocità prima dell'urto (Va)
Vb_t = Componente tangenziale della velocità dopo l'urto (Vb)

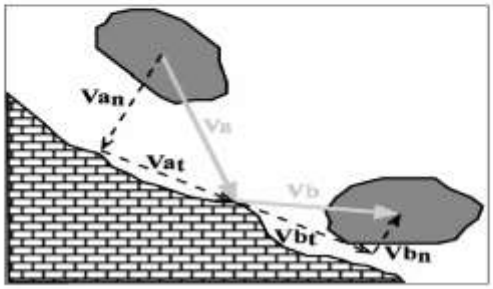

Figure 13: Relationship between a block's velocity before and after impact.

The value of the tangential return coefficient (Kt) is influenced by the vegetation cover, while the normal restitution coefficient (Kn) is determined by the elasticity of the impacting block surface.

The return coefficients are assigned to the slope ~~on which the boulders~~ through its ~~division~~ zonation into lithotechnically homogeneous units, i.e. cells in the topographic ~~reference~~ grid that possess the same type of substrate/cover. This geomechanical zoning operation is based on real differences in the geomorphology, vegetation cover and lithology of the slope terrain.

Unlike rebounding, the processes of rolling and/or sliding down the slope are phenomena that imply a considerable number of active forces of resistance that can be expressed collectively through the definition of a dynamic friction coefficient (Φ_d).

In the first simulations conducted for this work, reference parameters indicated in the literature were used for the two classes of terrain (**Table 2**) recognized on the Khinis side, namely: rock surface (calcareous bedrock, CB) and rocky terrain with a cover of shrub-like vegetation (SV).

After the model's input data (initial ~~departure~~ starting conditions, ~~and~~ elastic restitution and dynamic friction coefficients) have been defined, the probabilistic model used provides the following outputs:

- possible fall trajectories down the slope and ~~across~~ extension of accumulation areas;
- heights of fall trajectories (m) with respect to the slope surface;
- ~~specific~~ velocities and specific kinetic energies (m^2/s^2) acquired by dimensionless blocks along fall paths;
- maximum ~~block~~ run-out distances of rock blocks.

It should be remembered that the outputs of the model obtained with ROTOMAP refer to a kinematic (not dynamic) characterization of the rock–fall process, given the “dimensionless mass” assumption. In order to evaluate the energies involved and design effective countermeasures, a "design block volume" is then hypothesized, that is to say the volume of the most probable or largest block potentially affected by collapse phenomena.

	CALCAREOUS BEDROCK (CB)		
	Kn	Kt	φd
Broili (1973)	0.75-0.80 (K)		
Piteau e Clayton (1987)	0.65 - 0.75	0.8 - 0.9	
Budetta & Santo (1994)	0.20	0.53	
Azzoni & de Freitas (1995)	0.51-0.92 (K)		
Azzoni et al. (1995)	0.75-0.90 (K)		0.40-0.45
Chau et al., (2002)	0.40-0.60	0.65-0.90	
Guzzetti et al. (2003)	0.65	0.80	0.30
Guzzetti et al. (2004)	0.65	0.75	0.25
Ferrari et al. (2013)	0.60	0.80	0.20
~~mean~~ average min/max	0.573-0.674	0.744-0.811	0.287-0.30
~~mean~~ average (before calibration)	**0.623**	**0.777**	**0.293**
after calibration	***0.50***	***0.60***	***0.35***
difference	***19.24%***	***22.68%***	***16.28%***
	SHRUB-LIKE VEGETATION (SV)		
	Kn	Kt	φd
Pfeiffer & Bowen (1989)	0.30-0.33	0.83-0.87	
Pfeiffer & Higgens (1990)		0.82-0.85	
Agliardi & Crosta (2003)	0.33	0.75	0.50
~~mean~~ average min/max	0.315-0.33	0.80-0.823	0.50
~~mean~~ average (before calibration)	**0.315**	**0.812**	**0.50**
after calibration	***0.3***	***0.5***	***0.60***
difference	***14.28%***	***38.42%***	***16.67%***

Table 2. Published coefficients for the two types of terrain identified on the Khinis hillside. The values of these parameters obtained after *back analysis* model calibration and the differences with respect to the initial assumptions are also given.

5 RESULTS

5.1 Results of structural and geomechanical analyses

This section presents the results of the structural and geomechanical analyses conducted in the Khinis area in ~~accordance~~ agreement with the guidelines illustrated in § 3.2. For each analysis station (see **Figure 2** for location) a brief description of the types of mechanical discontinuity is given (illustrated by a stereographic projection plot). The data collected during the surveys in the field using the "scan line" method, which consists of measuring the discontinuities at regular distances along a horizontal reference line, are contained in Excel tables that are not included in this report but are available on request.

Station 1.

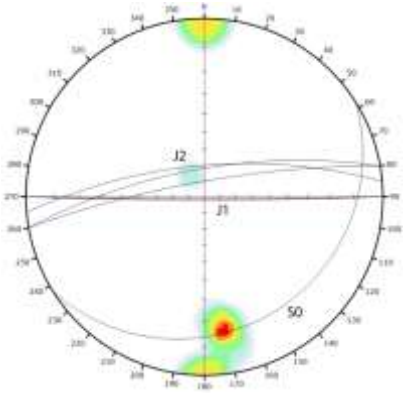

In Station 1 only two groups of discontinuities were observed, with dip directions to the S and NNW. Members of the first set (J1) are sub-vertical, and those in the second (J2) steeply inclined. The strata (S0) are gently inclined (16°) and dip roughly southeastwards (N146).

The few joint features ~~exemplars~~ measured ~~in~~ on the field ~~suggested~~ evidenced spacing~~s~~ of 1m for set J1 and 0.8-3.5m for set J2; the planes of both ~~continue~~ extend for one or several metres; the JRC varies from 6 to 8; the ~~plane~~ fracture surfaces show slight alteration (W2); with apertures of 1 – 3 mm they ~~are~~ can be classified as closed or semi-open fractures; they contain a fill of fine sand, and no signs of water infiltration were observed.

Station 2.

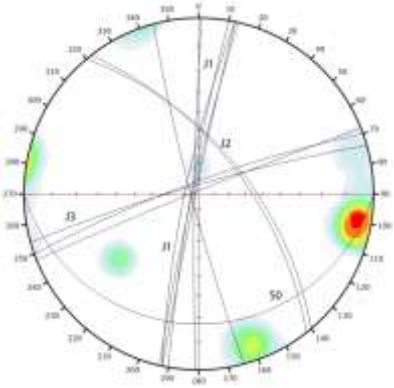

Station 2 ~~comprises~~ describes the discontinuities present at the base of the rock face that contains the large bas-relief. Three distinct groups of discontinuities are evident, J1-J3, all steeply inclined or sub-vertical. ~~Southwards running set~~ Set J1 ~~comprises~~ include planes with a WNW dip direction; set J2 dips towards NE; set J3 has a similar NNW dip direction ~~orientation~~ to set J2 of Station 1. The strata (S0) gently dip ~~only slightly~~ towards the south.

The discontinuities in set J1 show variable spacing (0.3-2.2m) and the other two medium spacing (0.3-0.4m); apart from a few exceptions, ~~their continuity~~ length is low, from 1 to 3 m; the JRC varies between 4 and 10; the surfaces are slightly altered (W2); small apertures mean that the surfaces are closed

(joint set 1) or semi-open (sets 2 and 3); fills are of fine sand. No signs of water infiltration were observed.

Station 3.

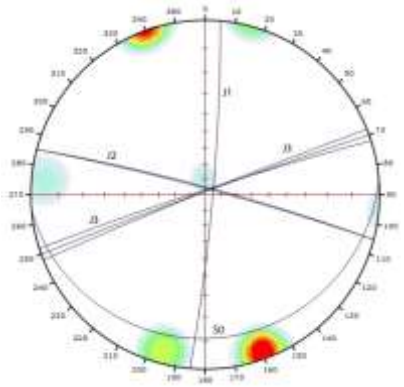

Station 3 is adjacent to the previous one and follows the base of the rock face containing the large bas-relief, where ~~it~~ this changes slightly in direction from N~~W~~E-~~SE~~ SW to ~~NNW~~NNE-~~SSE~~ SSW (**Figure 2**). Joints similar to those observed in Station 2 are present, though still fewer in number. Sets J1 and J3 resemble the same ~~categories~~ systems in Station 2, whereas J2 is rotated slightly anticlockwise, with a NNE dip direction ~~of NNE~~, not NE as at Station 2. The strata resemble those at previous stations. Discontinuity characteristics seem to change, with wider spacing (1-12 metres), ~~continuity~~ length up to 4m long, more marked surface alteration and wider gaps between the walls (1-80mm), filled mainly with fine sand produced by weathering of the calcarenit~~e~~ic rock. In several ~~instances~~ cases it was observed that the fill between discontinuity surfaces was damp and showed signs of leaching caused by the passage of water. For a height of 3 to 5 m above the surface of the ramp to the ex-quarry, the base of the rock face is karstified, with travertine deposits.

Stations 4 and 5

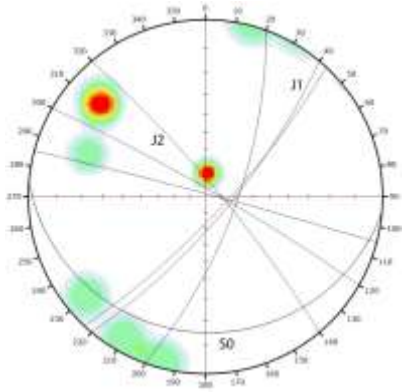

Stations 4 and 5 were sited in correspondence to the western side of the disused quarry area present at Khinis (**Figures 2a and 3a**), inside which Block A was identified (**Figure 2b**).

In this area, ~~in a~~ more evidently ~~fashion~~ than in the vicinity of the bas-reliefs, the weak deformation that affects the calcarenit~~e~~ic sequence ~~rock~~ is characterized by a few isolated mega-joints that are also clearly visible in the satellite image shown in **Figure 2** (NNE-SSW oriented discontinuity). These discontinuity features continue across most of the outcrop in ~~its~~ their vertical extension (25m) and are spaced several metres apart (**Figure 14**). This system (J1), which is sub-perpendicular to the hillside (~~and~~ that here has a dip direction of N35), ~~-~~is accompanied by a second (J2) joint system ~~-~~with a NW-SE orientation, parallel to the hillside, with steeply inclined discontinuities dipping to the NE.

The large fractures have high roughness (JRC from 8 to 16) and wide apertures – several metres in width towards the hill~~summit~~top but narrower toward the slope base. The upper portions of the discontinuities appear to contain no fill, whereas towards the base a coarse fill with a finer sandy matrix is often present. No signs of water

infiltration.

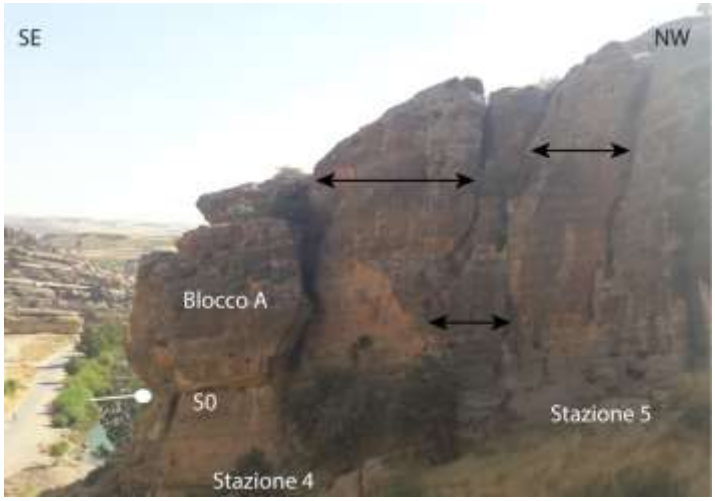

Figure 14. South-west side of the disused quarry (stations 4 and 5) with race faces interrupted by large mega-joints several metres in width (J1).

Station 6.

Station 6 is at mid-slope (altitude 480 metres) on the hillside above the large bas-relief and horseman bas-relief (**Figure 2b**). It corresponds to part of starting line 2 in the rock ~~-~~fall model~~e~~ing (**Figure 11**). Three distinct discontinuity groups are recognizable, in addition to the strata (S0). The first set (J1) includes the largest number of fractures, which ~~slope steeply,~~ run in a ~~direction~~ WNW-ESE direction and dip towards NNE; the second set (J2) is aligned NNW-SSE and dips towards WSW, comprising steep~~ly~~ ~~sloping~~ dipping joints as J1; the third set (J3) contains ENE-WSW-oriented and ~~-~~sub-vertical discontinuity planes.

These discontinuity systems show spacing of 1 to ~~circa~~ about 3 metres and ~~continue~~ extend for 1.5-3.0 metres (equal to the height of the small scarp (**see also Figures 4b and 9**). Roughness measurements give a JRC that varies greatly, from 5 to 20. The surfaces show little alteration, with aperture several tens of mm wide; the fill is of silty sand. No signs of water infiltration were observed.

Station 7.

Station 7 is sited near the ramp that leads up to the abandoned quarry, next to the river stream. In this area there is a clearly dominant joint system oriented NNE-SSW that dips towards ESE (J1); the components are largely sub-vertical and may be seen also on satellite photographs (**Figure 2**).

This set of discontinuities has similar properties to those measured in other sets found in stations 1-6: medium to wide spacing, roughness variable (2-18) but mostly high (12-18), little surface alteration, aperture widths of a few

cm, sand-silt filling, and no direct evidence of water infiltration.

Stations 1-7.

The overall ~~properties~~ setting of the ~~weak~~ fragile deformation field measured in the Khinis calcarenitice sequence are illustrate~~s~~d by means of a -"rosette" diagram. This diagram shows, on a horizontal plane represented by the (external) equatorial projection circle, a radial histogram that indicates - with arc segments - the density of the planes that intersect this horizontal surface.

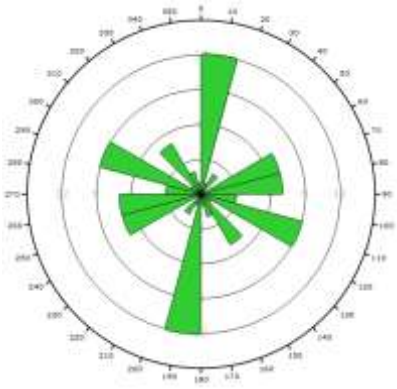

The radial limits of the arc segments correspond to the direction interval of the discontinuity planes (in this case 15-°). This diagram is thus a radial histogram showing fracture spatial density or frequency.

Approximately 60 discontinuity features were measured in the area, a relatively small number but commensurate with the characteristics of the weak deformation at Khinis, which shows few discontinuities within the rock mass. The greatest number of these have a NNE-SSW direction. A second set groups together those with direction varying between WNW-ESE and WSW-ENE, while a third smaller set are aligned NW-SE. Comparison of the results highlighted by the rosette diagram with the structural geology evidence obtained from photo-interpretation reveals a good correspondence between the deformation at the outcrop and slope scales (**Figure 2b**).

5.2 Results of discontinuity ~~resistance~~ strength parameter estimates

For the evaluation of the mechanical behaviour of discontinuities ~~in this work~~ the criterion developed by Barton and Choubey ~~is~~was used in this work, which through the definition of certain empirical parameters gives an estimate the of shear strength along the fracture planes on the basis of the formula (mentioned above):

$$\tau' = \sigma'_n \cdot \tan\left[JRC \cdot \log_{10}(JCS/\sigma'_n)\right]$$

The value of JCS may be obtained from sclerometric measurements. **Tables 3 and 4** furnish a (partial) example of the measurements taken at stations 6 and 7, respectively (where outcrop conditions permitted the use of the Schmidt Hammer), on one of the ~~joint~~ discontinuity systems recorded in the stratigraphic sequence ~~(~~ and S0~~)~~.

St 6																						corre~~c~~cted.
	1		2		3		4		5		6		7		8		9		10		tot/8	
J1	n°	or.	n°	or.	n°	or.	n°	or.	n°	or.	n°	or.	n°	or.	n°	or.	n°	or.	n°	or.		
r	32	horiz.	30	horiz.	30	horiz.	46	horiz.	37	horiz.	34	horiz.	30	horiz.	25	horiz.	20	horiz.	15	horiz.	**30**	**26.9**
R	40	horiz.	39	horiz.	38	horiz.	35	horiz.	34	horiz.	29	horiz.	38	horiz.	28	horiz.	34	horiz.	33	horiz.	**35**	**31.9**

ha formattato: Tipo di carattere: (Predefinito) Times New Roman

ha formattato: Tipo di carattere: (Predefinito) Times New Roman

ha formattato: Tipo di carattere: (Predefinito) Times New Roman

	1		**2**		**3**		**4**		**5**		**6**		**7**		**8**		**9**		**10**		**tot/8**	
S0	n°	or.	n°	or.	n°	or.	n°	or.	n°	or.	n°	or.	n°	or.	n°	or.	n°	or.	n°	or.		
r	45	90b	43	90b	44	90b	47	90b	47	90b	47	90b	44	90b	46	90b	47	90b	38	90b	**45**	
R	44	90b	52	90b	48	90b	49	90b	48	90b	45	90b	47	90b	45	90b	45	90b	42	90b	**46**	

Table 3. Sclerometric measurements taken at Station 6. Legend: n°=number of Schmidt Hammer rebounds; or. = hammer orientation (horiz=horizonthal; 90b=90°downwards). Extreme values excluded from the calculation are shown in red.

St 7																						corrected.
	1		**2**		**3**		**4**		**5**		**6**		**7**		**8**		**9**		**10**		**tot/8**	
J1	n°	or.	n°	or.	n°	or.	n°	or.	n°	or.	n°	or.	n°	or.	n°	or.	n°	or.	n°	or.		
r	40	horiz.	34	horiz.	39	horiz.	32	horiz.	38	horiz.	42	horiz.	34	horiz.	28	horiz.	35	horiz.	36	horiz.	**36**	**32.9**
R	36	horiz.	28	horiz.	44	horiz.	40	horiz.	40	horiz.	44	horiz.	36	horiz.	34	horiz.	44	horiz.	39	horiz.	**39**	**36.3**
	1		**2**		**3**		**4**		**5**		**6**		**7**		**8**		**9**		10		**tot/8**	
S0	n°	or.	n°	or.	n°	or.	n°	or.	n°	or.	n°	or.	n°	or.	n°	or.	n°	or.	n°	or.		
r	40	90b	36	90b	44	90b	38	90b	35	90b	38	90b	28	90b	40	90b	40	90b	39	90b	**38**	
R	42	90b	37	90b	48	90b	40	90b	37	90b	38	90b	42	90b	42	90b	37	90b	37	90b	**45**	

Table 4. Sclerometric measurements taken at Station 7. For legend see Table 3

Taking into consideration the Scmidt Hammer results obtained at stations 6 and 7 on the ~~main~~ all joint surfaces (i.e. not just those of the systems shown in **Tables 3 and 4**), the correlation chart shown in **Figure 9** gives an average JCS value of 42 MPa. This value, in the absence of other available measurements due to the inaccessibility of the rock faces elsewhere, was extrapolated to other areas of the study zone and taken to be representative of the discontinuities affecting the Khinis calcarenite~~ic succession~~sequence. In a similar ~~fashion~~way, the average JCS value for the bedding ~~layer~~ surfaces (S0), throughout the study zone, was taken to be 60 MPa, in correspondence with the highest rebound ~~readings~~ numbers obtained with the ~~instrument~~Schmidt Hammer.

In contrast, for the JRC parameter site-specific values were considered due to the higher number of in situ measurements available.

Lastly, from the formula proposed by **Barton and Choubey (1977)** for estimation of the residual friction angle ~~of attrition~~ φ_r for a generic altered discontinuity joint, i.e.:

$$\phi_r = (\phi_b - 20°) + 20\,(r/R)$$

the basic angle of attrition (φ_b) for a calcarenite was taken as 30°, and φr values varying between 27° and 28° were estimated. Then, for a greater safety margin, the minimum value of 27 ° was used and – as in the case of the JCS value – extrapolated to the entire area. A slightly higher figure, 30°, was obtained for stratum surfaces.

ha formattato: Pedice

ha formattato: Pedice

5.3 Results of limit~~ing~~ equilibrium method analysis for ~~stability analyses for~~ blocks A and B stability

This section gives the results of the stability analyses performed with the equilibrium method analysis for the two blocks A and B described above. **Table 5** summarizes, for each block, the slope geometry, rock block dimensions obtained from the geometrical intersection of the discontinuities recorded in the field, rock block geometry and the dynamic equilibrium conditions.

Block A		**Block B**	
Slope geometry			
Slope Height	20m	Slope Height	18m
Slope Angle:	83°	Slope Angle:	84°
Rock block dimension			
Wedge Height	20m	Wedge Height	12m
Wedge Length	10m	Wedge Length	11.5m
Wedge volume	880m^3	Wedge volume	700m^3
Wedge Weight:	19.41 MN	Wedge Weight:	16.215MN
Rock block geometry			
Failure Plane Angle	52°	Failure Plane Angle	17° (=S0)
Upper face width:	5.30m	Upper face width:	5m
Tension Crack Length	12.23m	Tension Crack Length	10.39m
Failure Plane length	10.86m	Failure Plane length	6.4m
Dynamic condition			
Driving force	15.30MN	Driving force	4.71MN
Resisting force	18.9MN	Resisting force	13.16MN
Factor of safety (Fs)	1.24	Factor of safety	2.59

Table 5. Summary of geometry, dimensions and dynamics of analyzed blocks A and B.

5.3.1 Block A

Block A, located at the south-west margin of the disused quarry area, has a prismatic shape and is bounded to the rear by a combination of a sub-vertical tension crack and a less steep failure plane which together cut off the entire ~~calcarenite succession~~ rock outcrop from the top to the bottom of the slope (**Figures 15 and 16**).

The block's length is about 10 metres, its height up to 20 metres, and its width estimated at 4 to 5 metres. Considering the form and inclination of the delimiting surfaces, its volume is estimated to be about 900 m^3. The failure mechanism would be planar sliding on the slippage surface, which might also result in secondary toppling. Its stability is precarious, as highlighted by the safety ratio Fs = 1.~~43~~24 between the resisting and driving forces, calculated using ~~-~~a limiting equilibrium approach.

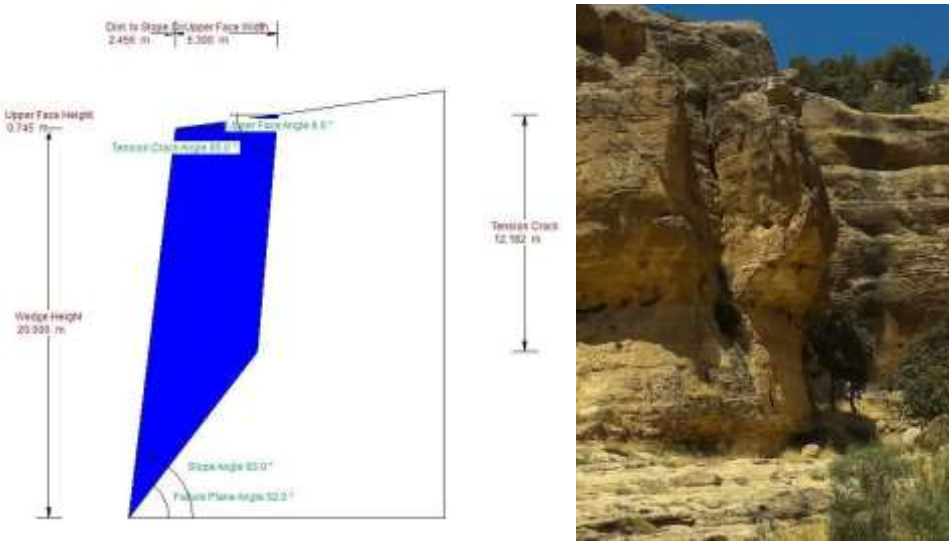

Figure 15. 2D geometrical reconstruction of Block A, located on the south-west side of the disused quarry (right).

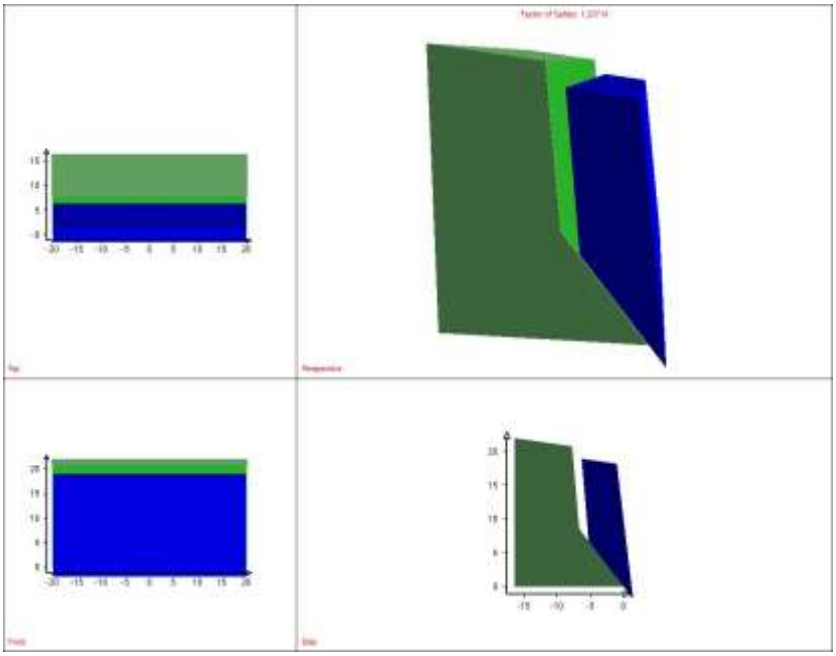

Figure 16. 3D geometrical reconstruction of Block A.

Block A's detachment from the rock wall and its consequent collapse could be caused by two different triggering factors: seismic vibration, or an increase in interstitial water pressures along the boundary discontinuities caused

by very heavy rainfall.

Figures 17 and **18** show the results of "sensitivity" analyses of the block-slope system, which highlight the variation of the instability conditions (Fs) ~~as~~ following the ~~size~~ intensity of the seismic input ~~and~~ or interstitial water pressure increase~~s vary~~.

The action of seismic shaking is expressed by a "seismic coefficient", a dimensionless number that defines the seismic acceleration as a fraction of the acceleration due to gravity. Typical values of the seismic coefficient range from 0.1 to 0.4g. If a_g = seismic coefficient, g = acceleration due to gravity (= 9.81 m/s^2) and m = mass of sliding block, the seismic force applied to the block in a horizontal direction may be expressed as F = m a_g g. In the case of Block A conditions of instability (Fs<1) are reached after a seismic event with a modest 'a' value, equal to 0.12g (**Figure 17**)

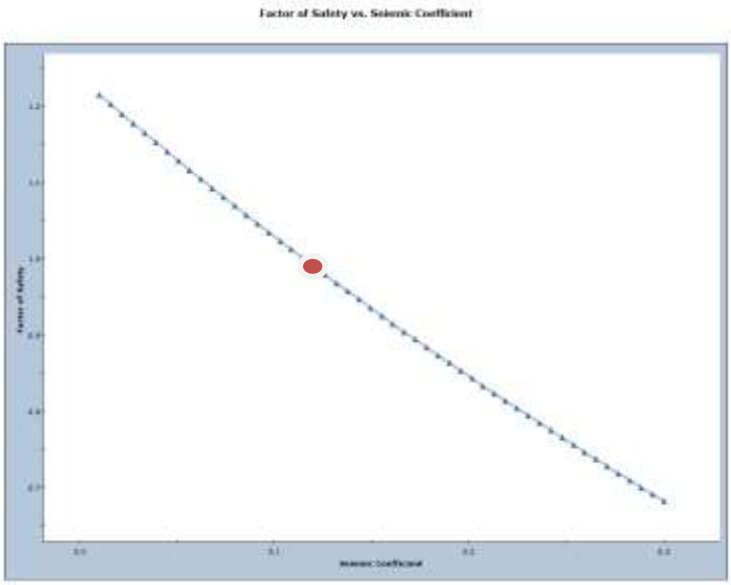

Figure 17. Sensitivity analysis of the Block A-slope system with respect to seismic movement expressed as a_g.

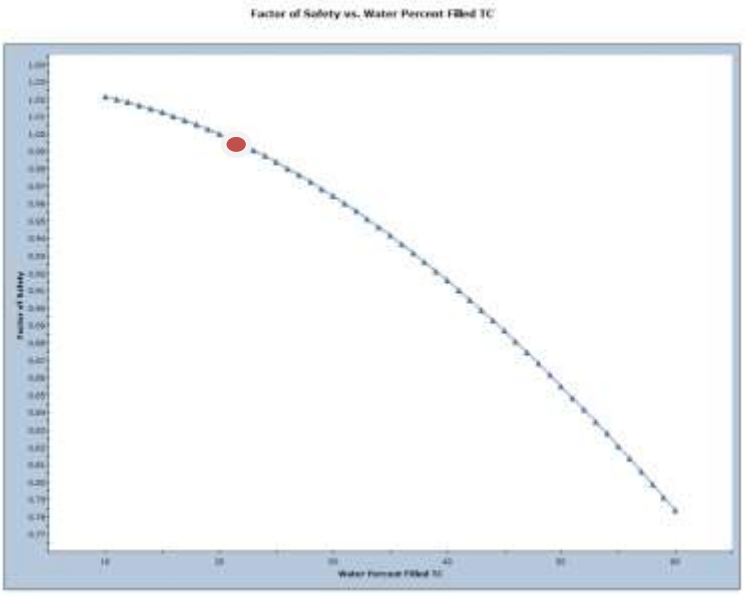

Figure 18. Sensitivity analysis of the Block A-slope system with respect to interstitial water pressure increase.

To include water pressure increase in the stability analysis of Block A, a theoretical distribution model was adopted that gives the maximum (peak) value of the water pressure at the base of the tension crack. To make the block unstable, it would be enough for circulating water to fill the tension crack to a proportion of 21%.

5.3.2 Block B

Block B is a parallelepiped in shape and its height is less than that of the slope; the potential sliding surface, which coincides with the ~~stratification~~ bedding plane (S0), reaches the surface at about a third (6m) of the overall slope height (18m). The resulting wedge therefore has a residual height of about 12 metres, a length parallel to the rock face of 11.5 metres and a width of about 5 metres. ~~-~~Considering the shape of the block, its estimated volume is about 700 m^3 (**Figures 18 and 19**).

In similar ~~fashion~~ mode to Block A, the potential failure mechanism for Block B is planar sliding, in this case along the ~~stratification~~ bedding ~~surface~~. ~~Movement~~ Detachment ~~is~~ would be allowed by a tension crack to the rear, which however has different characteristics with respect to Block A – where the tension crack is well developed and even more than one metre wide. In the case of block B, the fracture behind that could free it from the rest of the rock face is discontinuous and in some sections still closed. The limit~~ing~~ equilibrium calculation model shown in **Figures 19 and 20** makes the simplifying assumption that the tension crack is fully developed, from the top of the slope to the intersection with the plane of slippage. ~~and t~~The safety factor calculated (Fs = 2.59) is therefore an underestimate. The block is basically stable (**Table 5**).

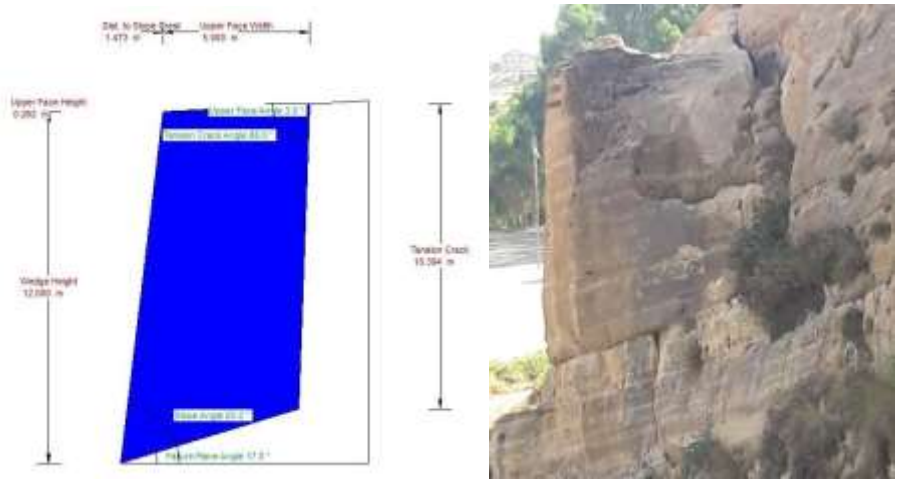

Figure 19. 2D geometrical reconstruction of Block B~~,~~ containing bas-reliefs ~~located on the SW side of the disused quarry~~ (right).

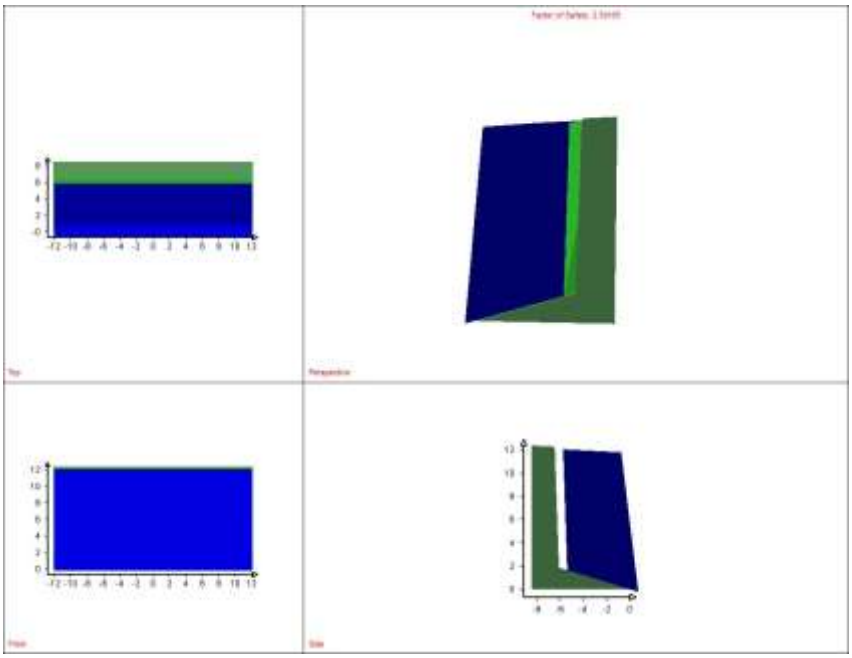

Figure 20. 3D geometrical reconstruction of Block B, containing bas-reliefs

These conditions of stability would be compromised (Fs <1) only by an exceptional seismic event with a value of a_g higher than 0.4g (**Figure 21**). ~~-~~Considering, on the other hand, ~~increased~~ the interstitial water pressure as a potential cause of collapse, ~~in modelling the limiting equilibrium~~ an ~~model~~ assumption was ~~used~~ made that foresees its ~~development~~ increase on the lower slippage surface corresponding to the ~~stratification~~ bedding plane~~,~~ (since the tension crack is partially sealed). To reach conditions of instability the slippage surface would have to be 70% full, producing a marked increase in interstitial pressure (**Figure 22**).

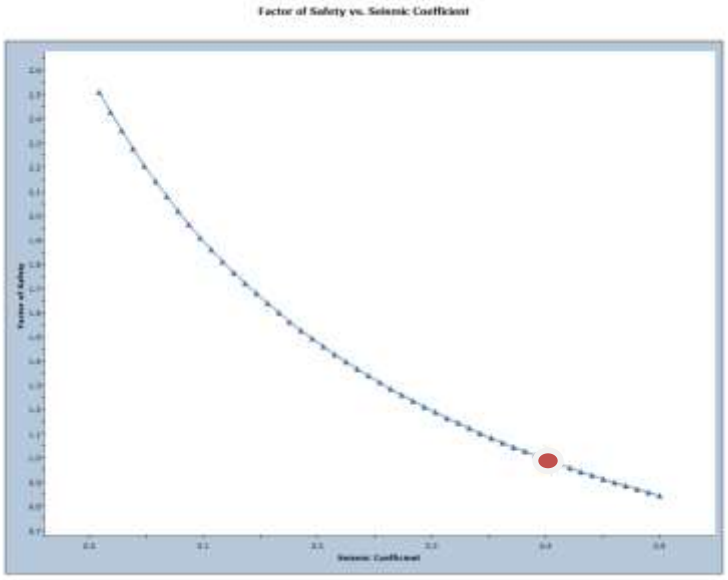

Figure 21. Sensitivity analysis of the Block B-slope system with respect to seismic movement expressed in terms of a_g

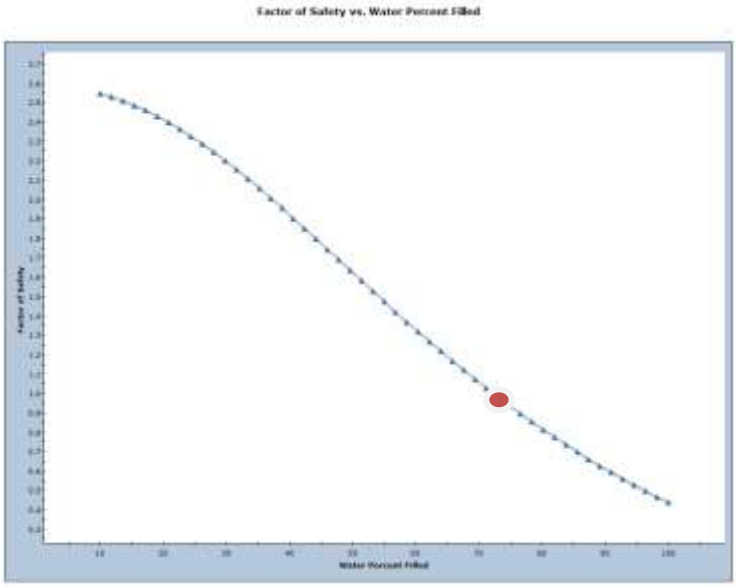

Figure 22. Sensitivity analysis of the Block B-slope system with respect to interstitial pressure increase.

5.4 Results of probabilistic modelling of rock-fall processes

The ~~entire process of~~ probabilistic and kinematic modelling of rock-fall processes was ~~conditioned~~ constrained by ~~field measurements consisting of~~ an inventory of observ~~able~~ed fallen boulders in situ. **Figure 23** shows the spatial distribution of 83 calcarenite~~ic~~ boulders located by photo-interpretation of satellite images and during ~~work in the~~ field work. In the course of their descent, 54 of the surveyed ~~boulders~~ rock blocksstopped on the ~~same~~ inclined slope without reaching the valley floor; 29 others reached the valley floor and stopped there. This latter figure should not be considered representative of the phenomenon, since some blocks may have been removed or have fallen into the river (and are thus no longer discernible).

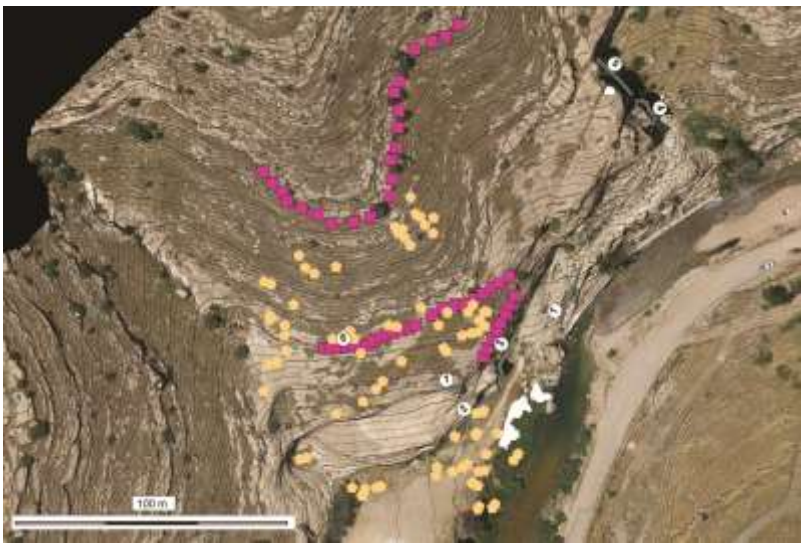

Figure 23. ~~Boulder~~ Rock block inventory (orange pentagons), starting points (red squares), and structural analysis scan lines

From the starting points (68) located by the model at the base of the scarps the fall of blocks was simulated with initial minimum and maximum velocities of 4.1 and 5.75 m/sec (in ~~accordance~~ agreement with the equation $V_0=Cs\sqrt{2g\cdot H}$ and using Cs=0.75 for sub-vertical faces Hmin, Hmax = 1.5, 3m). Moreover, a symmetrical angular deviation of 15° from the line of maximum slope of the hillside was specified. The number of simulations obtained was equal to (68)·(2)·(2) = 272.

Figure 24 shows the geomechanical zoning, with reference to the two recognized terrain classes and their spatial distribution on the slope and in the valley bottom area. For parameters Kn~~.~~, Kt and Φ_d ~~Kt and Φd~~ see also **Table 2**. The stream area has also been artificially added; very low return coefficients and very high friction values were assigned to ensure that boulders that reach the riverbed stop there.

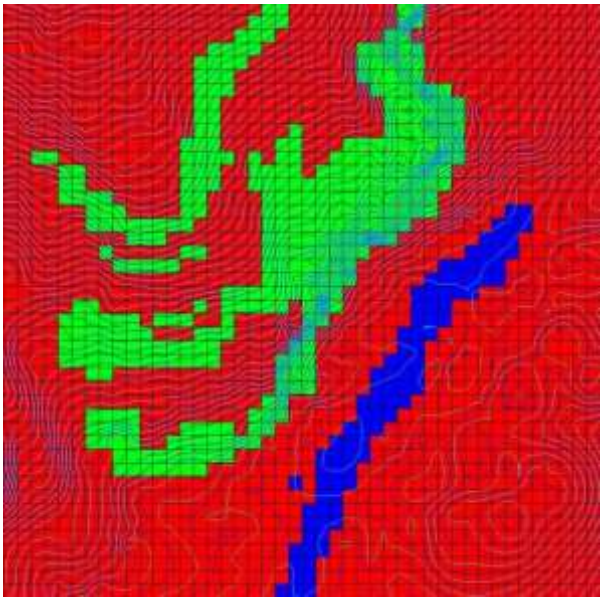

Figure 24. Geomechanical zoning of the slope and initial pre-calibration parameters; rock outcrops in green (Kn;Kt;Φ_d=0.62;0.77;0.29), rocky terrain with shrub cover in red (Kn;Kt;Φ_d = 0.31;0.81;0.50), the stream in blue (Kn;Kt;Φ_d = 0.2;0.2;0.99); 5m grid.

By gradually varying the elastic ~~return~~ restitution and dynamic friction parameters, and keeping the initial motion parameters (V_0, scarp position and height) constant, we passed through 5 model calibration ~~(or back analysis)~~ steps, finally obtaining a simulation of the trajectories that accords with the ~~boulder~~ rock blocks distribution recorded in the inventory (80% of observed boulders inside ~~stopping~~ arrest areas predicted by the model), as shown in **Figure 25**. The changes made to the elastic restitution and friction parameters to obtain this result were not significant, always less than 25% of the initial value except for one non-negligible reduction, equal to 38.42%, of the Kt value for the terrain category that includes bedrock covered by shrubby vegetation (**Table 2**). It proved necessary to effect this reduction in the tangential elastic return coefficient in order to obtain results that were congruent with the ~~boulder~~ rock block inventory. This fact might be explained by assuming that the vegetation, where present, played an important role in arresting the motion of the boulders ~~in descent~~.

Figure 26 summarizes the results obtained ~~using the model~~ and shows the 272 simulated trajectories. In the middle and upper parts of the slope, above the rock faces with the bas-reliefs, descent occurs mainly by rotational slipping (sections in green) and only after passing beyond the major break in the slope do rebound (and flight) phases prevail (sections in red). Overall, the trajectories show weak angular dispersion, in accordance with the regularity of the local topography.

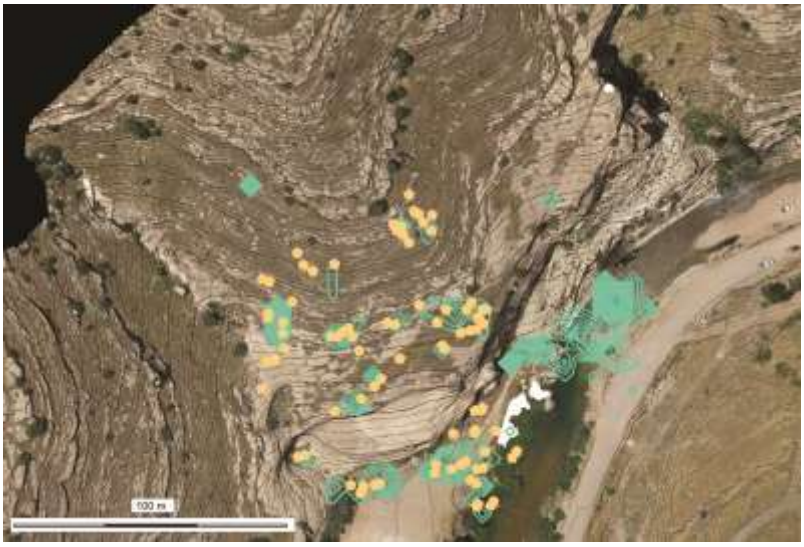

Figure 25. Comparison between the last modelling step and the ~~boulder~~ rock block inventory.

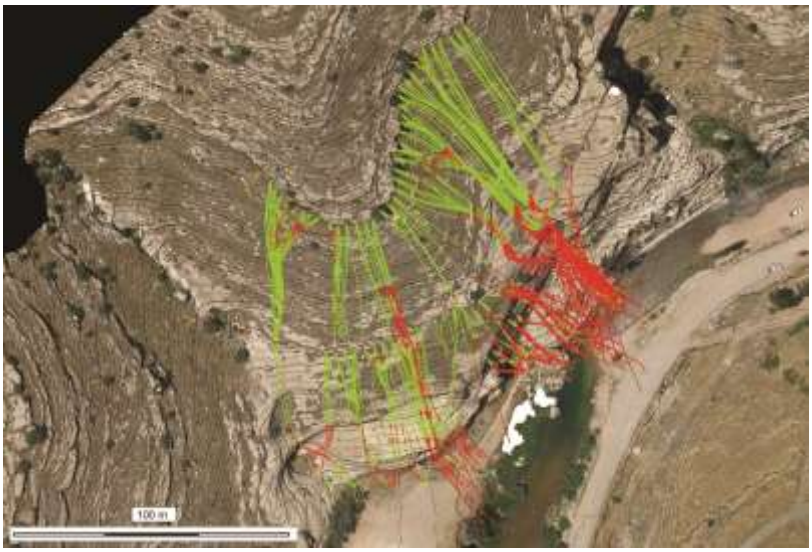

Figure 26. Simulation of the 272 ~~descent~~ trajectories; rotational sliding sections in green; rebounds (flights) in red.

ROTOMAP modelling of rock fall processes also enabled visualization of spatial distribution on the slope, from the starting areas to the ~~stopping~~ arrest areas, of the kinematic parameters ~~of the motion~~ of the "dimensionless"

falling boulders, namely their speed, specific kinetic energy (Ecin=1/2v^2, measured in m^2/sec^2) and rebound heights (measured in metres). For each of the 272 descents the model calculated the values of these quantities along the trajectories – as can be seen for example in **Figure 27**, which represents descent n° 172 (along which very high values of specific kinetic energy and height are registered). By means of spatial interpolation ~~of the values of the 272 trajectories,~~ the model reconstructed the spatial distribution of motion parameters, illustrated in **Figures 28 and 29**.

The specific kinetic energy values (**Figure 28**) are quite low on the upper part of the slope, where they do not exceed 50 m^2/sec^2, whereas they increase towards 100 m^2/sec^2 when the boulders approach the edge of the main scarp. After the last rebound, the free-fall phase from the Khinis scarp leads to a marked increase in kinetic energy, since friction is practically absent. High velocities are reached, with energies of up to 277 m^2/sec^2.

The distribution of ~~boulder~~ rock blocks heights in the rebound phases is shown in **Figure 29**, where contours are only shown for values of h> 1m. In ~~accordance~~ agreement with what is shown in **Figure 26**, where there is a marked prevalence of ~~rotatory~~ sliding sections in the upper and middle parts of the slope, the heights reached by the blocks are very ~~small~~low. On the western side of the slope heights are less than ~~one metre~~1m for long stretches, and never exceed 5m, a value reached during the flight phase from the main scarp at the middle of the slope. The same can be said for the eastern side of the slope, where high values (11-14m) are recorded only for the flight phase following the edge of the main scarp.

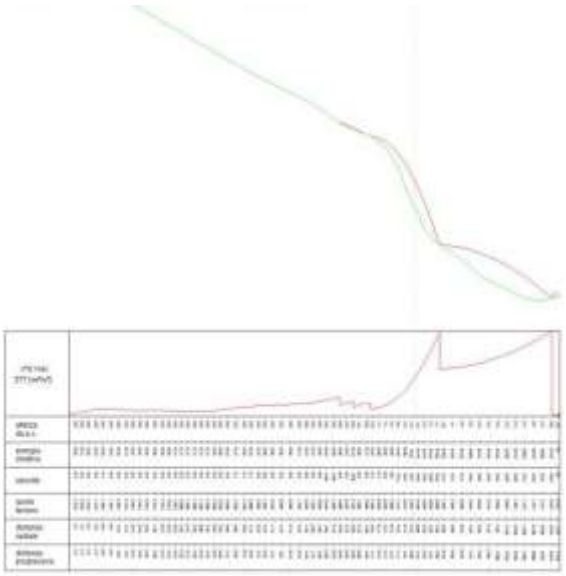

Figure 27. Down-slope progression of rock-fall motion parameters for one of the 272 modelled ~~descents~~trajectories.

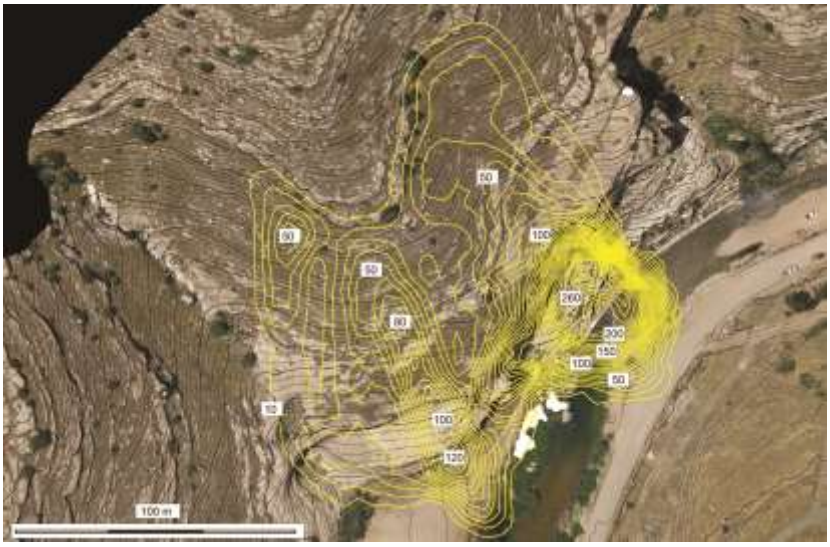

Figure 28. Spatial distribution of specific kinetic energy values (m^2/sec^2) on the Khinis hillside.

Figure 29. Spatial distribution of rebound height h (expressed in m) on the Khinis hillside (for h>1m).

5. DISCUSSION OF RESULTS AND PROPOSALS FOR MITIGATION OF LOCAL HYDROGEOLOGICAL INSTABILITY.

In order to define a plan to mitigate the geological instability caused by rock-fall processes in teh Khinis area it is necessary to implement the kinematic model in a complete dynamic simulation that also takes into account the volumes (and therefore the masses) of the stone blocks in motion down the slope.
To this end it is necessary establish the properties of a "design block", that is to say a theoretical block corresponding to – or larger than – the most likely block that might potentially detach from the rock faces and move down the slope as far as the stopping areas.
In the case of Khinis the dimensions of the design block were determined on the basis of the results of the structural and geomechanical analysis conducted in Station 6, corresponding to part of starting line 2 (**Figures 2, 4a-c**). From the study of the geometric relationships between the various joint systems ~~present on this slope~~, a maximum reference volume of 4.5 m^3 was obtained, representing a squat columnar block 2 metres high, and 1.5 metres wide and deep (**Figure 30**). The volume of the design block adopted is related to the maximum spacing between the joint systems observed at Station 6 and does not take account of the process of block fragmentation that usually follows detachment from the scarp face. In any case, an overestimated design block size, once included in the model used to calculate the energies involved (and the scale of the necessary countermeasures), is an added safety feature.

Figure 30. Assessment of a design block at Station 6.

Following the choice of the design block, protection measures must be devised in order to mitigate the risk associated with local rock-fall processes, which at Khinis might consist of the installation on the slope of rockfall barriers whose purpose is to stop the movement of blocks; the calculations needed to establish the dimensions of

such constructions are shown in **Table 6**.- Starting from the volume proposed (4.5m^3), the design block's mass is calculated – using a density of 2400 kg/m^3 for the calcareniteic rocks that characterize the Khinis sequence.- which gives an estimate figure of 10,800 kg (10.8 t). The design block mass is then multiplied by the specific kinetic energy (m^2/sec^2) indicated by the ROTOMAP simulation for the location in which the rockfall barrier will be installed. It is clearly preferable to place the barriers in sites where the specific Ecin values are lower (**Figure 31**). In terms of dimensions the calculation corresponds to 1kg·1m/s^2·1m = 1N 1m=1J and shows how much work is needed to arrest a boulder's descent. **Table 6** lists the impact energy values envisaged by the modelling for the slope sectors where it is planned to position the 8 protective barriers, each 30 metres in length; these are placed sub-parallel to the slope and ensure portions of linear overlap (**Figure 31**).

	V (m^3)	Mass (kg)	Weight (N)	Max Ecin$_{max}$ (m^2/s^2)	Impact Energy (KJ)	Barrier energy (KJ)	Barrier height (m)
DB	4.5	10800	105948				
BARRIER 1				**50**	540	1000	3
BARRIER 2				**50**	540	1000	3
BARRIER 3				**40**	432	500	2
BARRIER 4				**50**	540	1000	3
BARRIER 5				**30**	324	500	2
BARRIER 6				**40**	432	500	2
BARRIER 7				**30**	324	500	2
BARRIER 8				**40**	432	500	2

Table 6. Design block dimensions and Ccalculations of impact and absorption barrier energies for 8 elastic barriers assuming a design bock (DB) of 4.5m^3.

ha formattato: Apice

The installation of these rockfall barriers would thus interrupt the 272 trajectories of a hypothetical design block 4.5m^3 in volume falling down the slope (**Figure 31**).

The size of the barriers and their capacity to absorb energy ('barrier energy') was designed taking into account the largest maximum Ecin and consequent impact energies modelled, again in the interests of safety (**Table 6**). In accordance with modern technical specifications, the rockfall barrier heights listed in **Table 6** correspond to the required absorption energies (e.g. **GeoBrugg**). In this regard, it should be noted that the proposal to locate the barriers in the upper-middle part of the slopes is also appropriate, since the motion of the falling boulders in these areas is largely due to roto-translation and they should not travel at heights of more than 1 metre above the ground (see **Figure 28**). This positioning of the barriers and their small size would have a limited impact on environmental and landscape conservation at the Khinis site, asand they would be far from the area of the bas-reliefs.

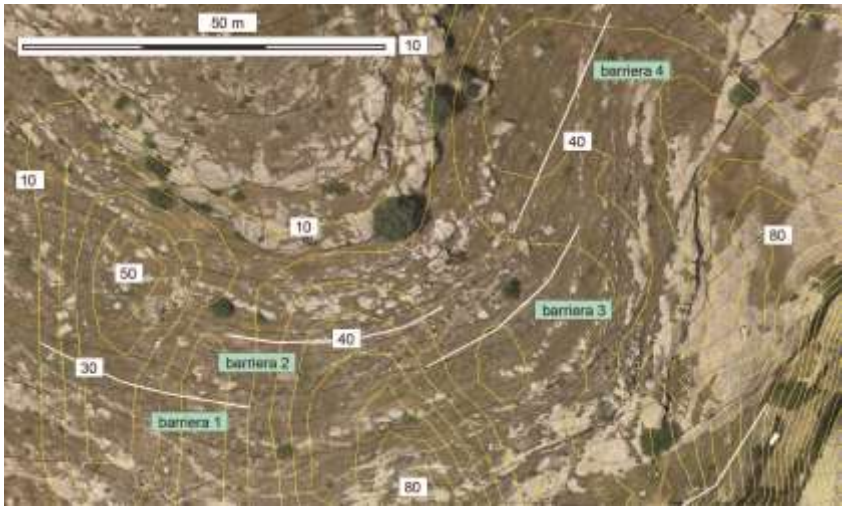

Figure 31. Proposed positions for the rockfall barriers based on specific Ecin values.

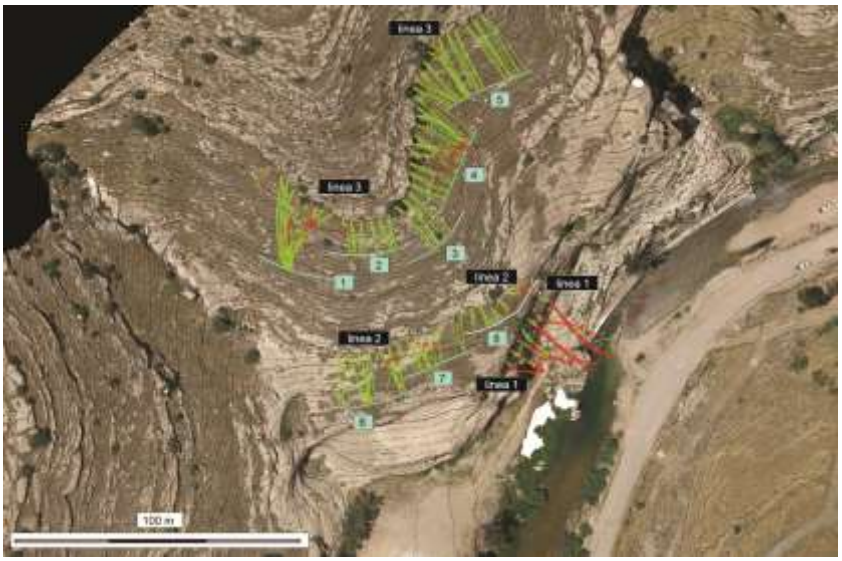

Figure 32. Results of dynamic modelling and the risk mitigation plan. In light blue, the 8 rockfall barriers.

Considerations that have little to do with the kinematic, and then dynamic, modelling of rock fall processes would

discourage the installation of rockfall barriers to stop the stone blocks that might potential fall from the lowest of the starting lines, line 1. This is close to the bas-relief, on the upper margin of the main scarp of the Khinis slope (**Figure 4b**). The visual impact of barriers here would be to the detriment of the site's landscape integrity. As a consequence, in **Figure 31** the simulated descents departing from line 1 are purposely not terminated. It is advisable to adopt a different solution here, that might involve the installation of supports such as ~~tie rods~~rock bolts ~~and the nailing of~~into blocks in evident conditions of instability and the simultaneous injection of cement mortars into the discontinuities that separate them from the rock mass. Alternatively, the controlled detachment of ~~certain~~ some rock ~~bodies~~ blocks should not be excluded.

ha formattato: Tipo di carattere: Grassetto

Analysis of the results of limit~~ing~~ equilibrium stability conditions for blocks A and B leads to different conclusions in these two cases, and to specific risk mitigation proposals for each.

For Block A, situated in the disused quarry and with a volume of circa 880 m^3, studies indicated a situation of imminent instability, summarized by a very low safety factor (Fs=1.24), which is due to the forces acting on the failure plane being close to the critical value of exceeding the resisting forces. Among possible factors that would trigger collapse are minor earthquakes, responsible for horizontal seismic accelerations equal to or greater than 0.12g, and meteorological phenomena that might not even be exceptional in terms of precipitation. Continuous monitoring with strain gauges or by modern remote-sensing techniques (terrestrial interferometry) is recommended in response to this condition of instability. Alternatively, a plausible strategy would be to plan the controlled collapse of the entire block ~~using explosives~~.

The situation of Block B containing the bas-reliefs, which has a volume of about 700 m^3, is decidedly less critical since the stability analyses show an Fs of 2.59, determined assuming the complete development of the tension crack behind it – which is not actually the case; Fs is therefore underestimated. Extremely intense triggering phenomena would be required to mobilize the entire mass of this block. Given the value of the bas-reliefs on the front surface, it would be advisable to make the conditions of this rock volume even more stable by clearing tree and shrub growth (that could widen the fissures over time) from the boundary discontinuity surfaces, and considering the injection of cement mortar or epox~~y~~idic resin to increase ~~its~~ ~~resistance~~strenght conditions.

In conclusion, it should be remembered that the results of a geological modelling depend on the scale factor, that is on the dimensions of the process under study, and on the observation capacity of the analytical tools.
The results of the probabilistic simulation model of rock-fall processes, although tied to field evidence and published data, cannot by their nature foresee all possible ~~descents~~ fall events and trajectories. At the same time the limiting equilibrium analyses presented in this report examined only two discrete blocks of rock that were identified on the wall of the Khinis escarpment. The possibility that other blocks, less clearly delimited by discontinuities or currently in apparently stable conditions, might suddenly collapse in response to calamitous

natural events has not been analyzed.

Lastly, it should not be forgotten that the limiting equilibrium analyses consider an undeformable rock mass, while the tensile/deformational conditions within the hillside could play a decisive role in giving rise to other types of gravitational instability and would require a different level of analysis.

In view of these considerations, in the final analysis it would be advisable to equip the Khinis site with a remote sensing system by positioning a modern terrestrial interferometer on the slope opposite that where the bas-reliefs are. This would make it possible to monitor over time the movements of different sectors of the slope, and to furnish an early warning system for the enaction of appropriate safety measures (controlled detachment of rock blocks, localized safety work, evacuation of the site).

BIBLIOGRAPHICAL REFERENCES

Azzoni A, de Freitas MH (1995) Experimentally gained arameters, decisive for rock fall analysis. Rock Mechanics and Rock Engineering, 28: 111-124. https://doi.org/10.1007/BF01020064.

Azzoni A, La Barbera G, Zaninetti A (1995) Analysis and prediction of rockfalls using a mathematical model. International Journal of Rock Mechanics and Mining Sciences 32: 709–724. https://doi.org/10.1016/0148-9062(95)00018-C.

Barton N, Choubey (1977) The shear strength of rock joints in theory and practice. Rock Mechanics 10: 1-54. https://doi.org/10.1007/BF01261801

Bourrier F, Dorren L, Nicot F, Berger F, Darve F (2001) Toward objective rockfall trajectory simulation using a stochastic impact model. Geomorphology 110(3-4):68–79. https://doi.org/ 10.1016/j.geomorph.2009.03.017.

Broili L (1973). In situ tests for the study of rockfall. Geologia applicata e idrogeologia 8: 105-111.

Bruce IG, Cruden, DM, Eaton TM (1989). Use of a tilting table to determine the basic friction angle of hard rock samples. Canadian Geotechnical Journal 26(3): 474-479. https://doi.org/10.1139/t89-060.

Budetta P, Santo A (1994) Morphostructural evolution and related kinematics of rockfalls in Campania (southern Italy): a case study. Engineering Geology 36: 197-210. https://doi.org/10.1016/0013-7952(94)90004-3.

Chau KT, Wong RHC, Wu JJ, 2002. Coefficient of restitution and rotational motions of rockfall impacts. International Journal of Rock Mechanics and Mining Sciences 39: 69-77 https://doi.org/10.1016/S1365-1609(02)00016-3.

Cruden DM, Hu XQ (1988) Basic friction angles of carbonate rocks from Kananaskis country, Canada Bull. Int. Assoc. Eng. Geol. 38: 55-59.

Del Maschio L, Gozza G, Piacentini D, Pizziolo M, Soldati M (2007) Previsione delle traiettorie dei blocchi mobilizzati da frane di crollo: applicazione e confronto di modelli. Giornale di Geologia Applicata 6: 33-44.

Ferrari F, Giani GP, Apuani T (2013) Towards the comprehension of rockfall motion, with the aid of in situ tests. Italian Journal of Engineering Geology and Environment 6: 163-171. https://doi.org/10.4408/IJEGE.2013-06.B-13.

GeoBrugg. Rock fall protection. https://www.geobrugg.com/en/Rockfall-Protection-77472.html

Gonzalez de Vallejo LI, Ferrer M, Ortuno L, Oteo C. (2005) Geoingegneria, Pearson Education Italia, 816 p. ISBN 13:978-88-7192-094-8.

Goodman, RE (1989) Introduction to rock mechanics. Wiley J and Sons, 2nd edition, New York.

Guzzetti F, Reichenbach P, Wieczorek GF (2003) Rockfall hazard and risk assessment in the Yosemite Valley, California, Usa. Natural Hazards and Earth System Sciences 3: 491-503. https://doi.org/10.5194/nhess-3-491-2003.

Guzzetti F, Reichenbach P, Ghigi S (2004) Rockfall hazard and risk assessment along a transportation corridor in the Nera Valley, Central Italy. Environmental Management 34: 191-208. https://doi.org/10.1007/s00267-003-0021-6.

Hoek E, Bray JW (1981) Rock slope engineering 3rd ed. The Institution of Mining and Metallurgy, London.

ISRM 2007. The Complete ISRM Suggested Methods for Rock Characterization, Testing and Monitoring: 1974–2006. Suggested Methods Prepared by the Commission on Testing Methods, International Society for Rock Mechanics, R. Ulusay & J.A. Hudson (eds), Compilation Arranged by the ISRM Turkish National Group, Ankara, Turkey, 628 pp.

Pfeiffer TJ, Bowen TD (1989) Computer simulation of rockfalls. Bulletin of the Association of Engineering Geologists 26: 135–146. https://doi.org/10.2113/gseegeosci.xxvi.1.135.

Pfeiffer TJ, Higgins JD (1990) Rockfall hazard analysis using the Colorado rockfall simulation program. Transportation Research Record, 1288, 117-126.

Piteau DR, Clayton R (1987). Computer rockfall model. In: ISMES (ed.). Proceedings of Meeting on Rockfall Dynamics and Protective Works Effectiveness, Bergamo, Italy, p. 123-125

Scioldo G (1991) Rotomap: analisi statistica del rotolamento dei massi. In: Guariso G. (ed.). Guida di informatica ambientale. Bologna, Patron, pp 81-84.

Scioldo G (2006) User guide: ISOMAP & ROTOMAP - 3D surface modelling and rockfall analysis. http://www.geoandsoft.com/english/download.htm.

Waltham AC (2009) Foundations of Engineering Geology, 3rd edn. Spon Press, Taylor and Francis, London